LANGUAGE-ENHANCED REPRESENTATION LEARNING FOR SINGLE-CELL TRANSCRIPTOMICS

Jiaqi Yang[1]**, Zhiyuan Liu**[2]**, Yaorui Shi**[1]**, Qingchuan Zhang**[1]**, Changhao Nai**[3]**,**
Junfeng Fang[2]**, Yahui Long**[4]**, Yang Zhang**[2]**, Xiang Wang**[1]
[1]University of Science and Technology of China [2]National University of Singapore
[3]Harbin Institute of Technology [4]Central South University
{acharkq,yaoruishi,zhangqingchuan32,naichh12,xiangwang1223}@gmail.com
{yangjiaqi20,fjf}@mail.ustc.edu.cn, longyahui@csu.edu.cn, zhang@nus.edu.sg

ABSTRACT

Single-cell RNA sequencing (scRNA-seq) offers detailed insights into cellular heterogeneity. Recent advancements leverage single-cell large language models (scLLMs) for effective representation learning. These models focus exclusively on transcriptomic data, neglecting complementary biological knowledge from textual descriptions. To overcome this limitation, we propose scMMGPT, a novel multimodal framework designed for language-enhanced representation learning in single-cell transcriptomics. Unlike existing methods, scMMGPT employs robust cell representation extraction, preserving quantitative gene expression data, and introduces an innovative two-stage pre-training strategy combining discriminative precision with generative flexibility. **Extensive experiments across nine datasets and five tasks show that scMMGPT significantly outperforms unimodal and multimodal baselines**. Notably, scMMGPT achieves relative improvements of **8.13%** for clustering on the COVID-19 dataset, **7.48%** for annotation on the Myeloid dataset, and **2.93%** for perturbation prediction on the Adamson dataset. Our code is available at `https://github.com/segmenttree9/scMMGPT`.

1 INTRODUCTION

Single-cell RNA sequencing (scRNA-seq) profiles gene expression at the level of individual cells, providing a fine-grained view of cellular heterogeneity (Saliba et al., 2014; Shalek et al., 2014; Silverman et al., 2020). The complexity and high dimensionality of scRNA-seq data necessitate powerful computational approaches that can leverage massive datasets efficiently and accurately (Angerer et al., 2017). Inspired by the success of large language models (LLMs) in natural language processing (Vaswani et al., 2017; OpenAI, 2023; Touvron et al., 2023a), specialized single-cell large language models (scLLMs) have emerged, leveraging self-supervised pre-training on extensive expression datasets to produce robust cell representations for downstream tasks such as cell annotation and clustering (Theodoris et al., 2023; Cui et al., 2024; Yang et al., 2022; Hao et al., 2024). However, existing scLLMs are mostly pre-trained solely on scRNA-seq data, inherently constraining the breadth of their cell representations.

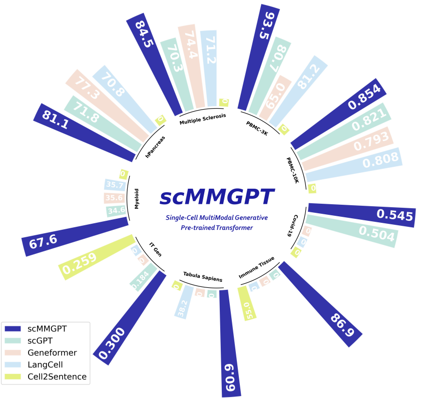

Figure 1: Performance of various scLLM on single cell tasks. We demonstrate results in cell type annotation, cell clustering, batch effect removal, cell description generation and pseudo-cell generation task. Detailed descriptions for metrics are provided in §E.4. Best viewed in color.

In this work, we explore **language-enhanced single-cell representation learning**, aiming to integrate the fine-grained molecular signals from scRNA-seq with the high-level biological knowledge encoded in textual descriptions and metadata. As Figure 2 shows, textual descriptions encode contextual information–such as species, tissue origin,

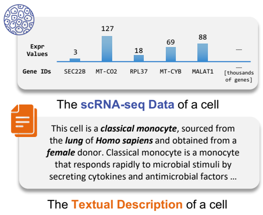
Expr Values
3
127
18
69
88
—
Gene IDs
SEC22B
MT-CO2
RPL37
MT-CYB
MALAT1
— [thousands of genes]
The scRNA-seq Data of a cell
This cell is a *classical monocyte*, sourced from the *lung* of *Homo sapiens* and obtained from a *female* donor. Classical monocyte is a monocyte that responds rapidly to microbial stimuli by secreting cytokines and antimicrobial factors ...
The Textual Description of a cell

Figure 2: Comparison between a cell's scRNA-seq representation and its textual description.

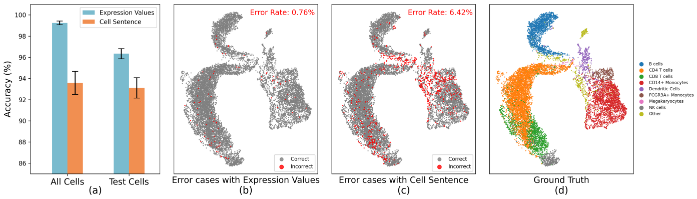

Figure 3: (a) Representing cells as cell sentences leads to significant accuracy degradation. (b-d) UMAP vis. of predicted cell types and ground truth. Prediction with cell sentences yields lower scores.

and cell type–that is not directly captured by expression profiles but is critical for downstream biological interpretation. Incorporating such textual knowledge offers a promising path toward more comprehensive and semantically meaningful cell representations.

To harness the rich biological knowledge in text descriptions for single-cell analysis, recent studies have explored joint cell-text modeling (Zhao et al., 2024; Liu et al., 2023b; Bian et al., 2024; Fang et al., 2025). However, we find that these efforts overlook key aspects of language-enhanced cell representation learning: **insufficient unimodal cell representation learning**, and **incomplete cell-text alignment**.
To address these gaps, we propose Single-Cell Multi-modal Generative Pre-trained Transformer (**scMMGPT**), a language-enhanced cell representation learning framework for single-cell transcriptomics. Rather than exploring chat-based interfaces with text LLMs (Fang et al., 2025; Levine et al., 2024; Schaefer et al., 2024), scMMGPT emphasizes improved performance in essential single-cell analysis tasks with information from the text modality. To ensure **robust cell representation learning**, scMMGPT preserves critical quantitative gene expression information during tokenization and employs contrastive pre-training with physiologically-motivated data augmentations. To achieve **comprehensive cell-text alignment**, scMMGPT incorporates two separate projectors for the bidirectional information sharing between scLLM and text LLM, and a comprehensive two-stage pre-training strategy with both discriminative and generative objectives.

With these breakthroughs, scMMGPT significantly surpasses existing unimodal and multimodal methods, establishing a new standard for leveraging textual knowledge in single-cell transcriptomics analysis. As shown in Figure 1 and the experiment section, **we demonstrate scMMGPT's performance across nine datasets and five downstream tasks.** Notably, the model achieves relative improvements of **8.13%** for clustering on the COVID-19 dataset, **7.48%** for annotation on the Myeloid dataset, **2.93%** for perturbation prediction on the Adamson dataset, and **28.41%** for cell description generation on the immune tissue dataset. Further experiments demonstrate its improvement for zero-shot cell type annotation. Finally, we perform comprehensive ablation studies to validate the effectiveness of scMMGPT's key components.

2 Related Works

Single-Cell LLMs. Single-cell sequencing technologies provide diverse biological features that facilitate the interpretation of cellular structures and functions (Heumos et al., 2023; Cao & Gao, 2022). Early efforts in scRNA-seq analysis focused on statistical approaches such as Seurat (Satija et al., 2015) and Harmony (Korsunsky et al., 2019). Advances in scRNA-seq have also generated massive, high-precision transcriptomic datasets, driving the development of Single-Cell LLMs (scLLMs) (Ziegenhain et al., 2017). This technique quantifies the mRNA molecule abundance, producing gene expression matrices that record expression values of individual genes across cells (Ji et al., 2021). Previous works have developed transformer-based foundation models on scRNA-seq data, pre-training with masked learning objectives on millions of cells (Zhao et al., 2023; Theodoris et al., 2023; Yang et al., 2022; Hao et al., 2024). Subsequent works improve the learning process by incorporating cell labels, such as batch information (Cui et al., 2024) and other cell metadata (Bian et al., 2024). After fine-tuning, these LLMs have proven useful in practical downstream tasks such as cell-type annotation, cell clustering, and batch effect removal.

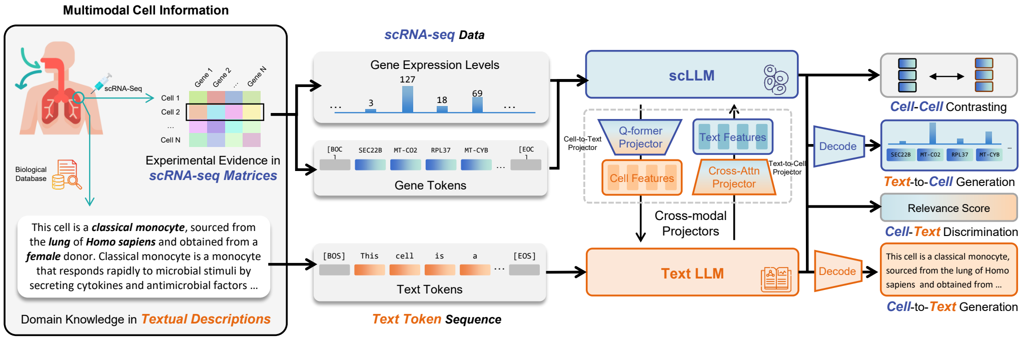

Figure 4: Overview of scMMGPT. (1) Cross-modal Discriminative Objective: Given paired cell and text inputs, the model learns to identify the correct textual description of a cell by aligning the outputs of the scLLM and text LLM. (2, 3) Cross-modal Generative Objectives: scMMGPT strengthens multimodal alignment through a unified generative pre-training strategy, jointly optimizing cell-to-text and text-to-cell translation tasks to facilitate bidirectional knowledge transfer.

Cell-Text Modeling. Incorporating free-text biological descriptions has proven useful for improving cellular representation learning, with prior works demonstrating that such auxiliary textual supervision can enhance the quality of cell embeddings (Chen & Zou, 2023; Liu et al., 2023b; Choi et al., 2024; Zhao et al., 2024). Beyond representation learning, enabling bidirectional translation between cells and text facilitates tasks such as universal cell-type annotation (Mao et al., 2025) and the generation of pseudo-cells (Luo et al., 2024a; Lopez et al., 2018). Recent efforts aim to build multimodal LLMs for single-cell data that align cell and text modalities directly (Fang et al., 2025; Schaefer et al., 2024). After instruction tuning on cell annotation or pseudo-cell generation, these models enable interactive single-cell analyses for human users. Nevertheless, the most crucial single-cell analysis tasks that boost real-world scientific discoveries rely more on efficient cell representation extraction to support tasks like cell annotation and clustering, which is often neglected in previous multimodal approaches.

Scientific Multimodal LLMs. Multimodal LLMs show remarkable potential for integrating data from various modalities (Li et al., 2023; Alayrac et al., 2022; Zhang et al., 2024), inspiring research for scientific modalities. Existing works have constructed multimodal LLMs for small molecules (Liu et al., 2023c; Fang et al., 2024; Liu et al., 2024a) and proteins (Xu et al., 2023b; Liu et al., 2024b) to tackle cross-modal scientific problems, such as description generation, molecular property prediction, and text-conditioned de novo design (Li et al., 2024; Edwards et al., 2022; Liu et al., 2023d; Cao et al., 2025; Liu et al., 2025; Luo et al., 2024b). Although single-cell analysis holds comparable scientific importance, the sparsity and high dimensionality nature of scRNA-seq data introduce a significant gap between transcriptomic and textual modalities, presenting challenges for joint modeling of them.

3 Method

To build scMMGPT, we first construct a diverse cell-text dataset to support cross-modal training (§3.1). Further, scMMGPT adopts a specialized scLLM that directly models original expression levels to bypass information loss, a pre-trained text LLM for generating descriptive annotations (§3.2), and bidirectional projectors to enable cross-modal information exchange. To facilitate comprehensive cell-text alignment and representation learning, we introduce a two-stage pre-training strategy (§3.3). After pre-training, scMMGPT can be applied to a range of downstream single-cell analysis tasks (§3.4). Figure 4 illustrates the overall architecture of scMMGPT.

3.1 Large Scale and Multi-Source Cell-Text Data Collection

Large-Scale Single-Cell Transcriptomics Collection. For single-cell transcriptomics data, we collect 60 million single-cell profiles from the biggest single-cell transcriptomics database Cellx-Gene (Program et al., 2025). The collected cellular data includes high-resolution scNRA-seq matrices with gene names and numeric expression levels and associated cell properties such as cell types, tissues, and disease statuses. To ensure data quality, we then conduct data filtering and deduplication (see Appendix B for more details). After these steps, we maintain scRNA-seq data of 27 million cells

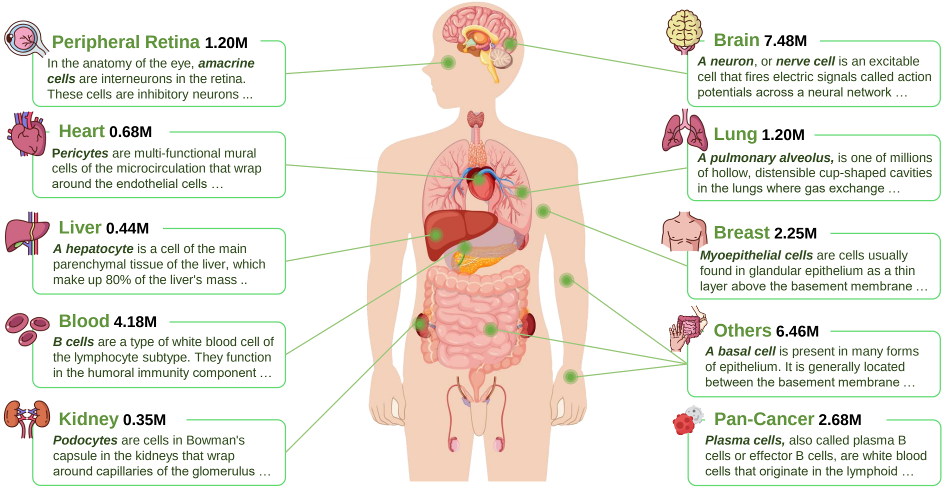
Peripheral Retina 1.20M
In the anatomy of the eye, amacrine cells are interneurons in the retina. These cells are inhibitory neurons ...
Heart 0.68M
Pericytes are multi-functional mural cells of the microcirculation that wrap around the endothelial cells …
Liver 0.44M
A hepatocyte is a cell of the main parenchymal tissue of the liver, which make up 80% of the liver's mass ..
Blood 4.18M
B cells are a type of white blood cell of the lymphocyte subtype. They function in the humoral immunity component …
Kidney 0.35M
Podocytes are cells in Bowman's capsule in the kidneys that wrap around capillaries of the glomerulus …
Brain 7.48M
A neuron, or nerve cell is an excitable cell that fires electric signals called action potentials across a neural network …
Lung 1.20M
A pulmonary alveolus, is one of millions of hollow, distensible cup-shaped cavities in the lungs where gas exchange …
Breast 2.25M
Myoepithelial cells are cells usually found in glandular epithelium as a thin layer above the basement membrane …
Others 6.46M
A basal cell is present in many forms of epithelium. It is generally located between the basement membrane …
Pan-Cancer 2.68M
Plasma cells, also called plasma B cells or effector B cells, are white blood cells that originate in the lymphoid …

Figure 5: Summary of data used in the pre-training of scMMGPT. The dataset includes 27 million single-cell transcriptomic profiles from diverse human organs and tissues.

across various human tissues, summarized in Figure 5. The diverse cell atlas ensures generalization and prevents scMMGPT from degenerating into overfitting specific tissues.

Large-Scale Cell Description Collection. For textual information, we gather free-form cell identity explanation (*e.g.,* definition of cell types and diseases) from two sources: (1) the OBO Foundry (Smith et al., 2007), which integrates professional reference for biomedical terms, and (2) Wikipedia, which contains comprehensible explanations of cell function. We construct textual descriptions of cells by merging the free-form cell explanations and the cell metadata from CellxGenes.

3.2 Neural Architecture for Language-Enhanced Cell Representation Learning

To leverage the strengths of both modalities, we utilize pre-trained models for unimodal cell representation learning and natural language generation. These models bring in domain-specific knowledge and robust in-domain feature extraction capabilities.

scLLM for Cell Representation Learning. To obtain high-quality cell representations, we employ scGPT (Cui et al., 2024), a state-of-the-art single-cell language model pre-trained on large-scale scRNA-seq data. Its architecture is tailored to jointly model gene symbols and their quantitative expression levels, which avoids the loss of information that occurs with ranked gene lists.

Each cell is represented as a vector derived from the raw count matrix $\mathbf{X} \in \mathbb{N}^{N \times M}$, where $\mathbf{X}_{ij}$ denotes the expression level of gene j in cell i. Since absolute gene expression values can vary across measurement platforms, we apply row-wise normalization before feeding into the model:

$$\tilde{x}_j^{(i)} = \log\left(1 + \frac{x_j^{(i)}}{\sum_{k=1}^{M} x_k^{(i)}}\right). \tag{1}$$

To mitigate data sparsity, we retain the top 2,048 most expressed genes per cell, which captures the majority of meaningful signals.

Text LLM for Text Generation. For the text LLM, we utilize LLaMA-2 7B (Touvron et al., 2023b), a decoder-only transformer that excels at text generation. Its extensive pre-training and generative architecture make it well-suited for biomedical text understanding and generation, such as describing cellular states. We tokenize the textual description of cells into a sequence of tokens $\mathbf{t}^{(i)} = [t_1^{(i)}, t_2^{(i)}, \dots, t_T^{(i)}]$ using the tokenizer in text LLM.

Bi-directional Projectors for Cell-Text Translation. To bridge the modality gap between cell and text LLMs, we introduce bidirectional cell-to-text and text-to-cell projectors that enable effective cross-modal alignment and information exchange.

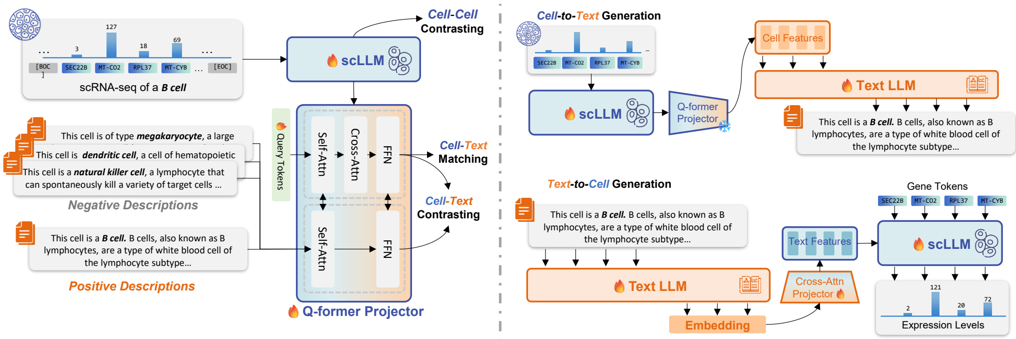
127
3
18
69
[BOC]
SEC22B
MT-CO2
RPL37
MT-CYB
[EOC]
scRNA-seq of a B cell
scLLM
Cell-Cell Contrasting
This cell is of type megakaryocyte, a large
This cell is dendritic cell, a cell of hematopoietic
This cell is a natural killer cell, a lymphocyte that can spontaneously kill a variety of target cells ...
Negative Descriptions
This cell is a B cell. B cells, also known as B lymphocytes, are a type of white blood cell of the lymphocyte subtype...
Positive Descriptions
Query Tokens
Self-Attn
Cross-Attn
FFN
Self-Attn
FFN
Q-former Projector
Cell-Text Matching
Cell-Text Contrasting
Cell-to-Text Generation
Q-former Projector
Cell Features
Text LLM
This cell is a B cell. B cells, also known as B lymphocytes, are a type of white blood cell of the lymphocyte subtype...
Text-to-Cell Generation
This cell is a B cell. B cells, also known as B lymphocytes, are a type of white blood cell of the lymphocyte subtype...
Text LLM
Embedding
Cross-Attn Projector
Text Features
Gene Tokens
SEC22B
MT-CO2
RPL37
MT-CYB
scLLM
121
2
20
72
Expression Levels

(a) Stage 1: Cross-modal *Discriminative* Pre-training

(b) Stage 2: Cross-modal *Generative* Pre-training

Figure 6: The two-stage cross-modal pre-training scheme. (a) In cross-modal discriminative pre-training, the model achieves cell-text integration by distinguishing matched cell-text pairs from unrelated pairs through contrastive and matching objectives. (b) In cross-modal generative pre-training, the model continues knowledge integration via unified generative tasks, including cell-to-text and text-to-cell generation objectives.

- **Cell-to-text projector** is implemented with a Query Transformer (Q-Former) (Li et al., 2023) with 32 learnable queries, which maps high-dimensional cell embeddings from the scLLM into the token embedding space of the Text LLM. We initialize the Q-Former with weights from BiomedBERT (Gu et al., 2021), a BERT encoder trained on PubMed abstracts and biomedical literature (Canese & Weis, 2013).
- **Text-to-cell projector** is realized using cross-attention layers (Vaswani et al., 2017) that project LLaMA-2 output embeddings into the hidden space of scGPT. The resulting representations are used as soft prompts (Li & Liang, 2021), conditioning the scLLM for text-to-cell generation.

3.3 Comprehensive Pretraining for Cell-Text Alignment and Cell Representation Learning

We adopt a two-stage pre-training strategy to pretrain cell representation, inject textual knowledge into the scLLM, align modalities, and enable bidirectional cell-text generation. Stage 1 aligns the representations and achieves coarse-grained knowledge injection through joint **cross-modal discriminative pre-training** and **contrastive cell representation learning.** Further, Stage 2 enables bi-directional cell-text translation via **generative pre-training**.

Stage 1: Cross-modal discriminative pre-training. We conduct cross-modal discriminative pre-training to create a shared latent space that captures semantic correspondences between scRNA-seq profiles and biomedical texts. Given a normalized single-cell expression vector $\widetilde{\mathbf{x}}^{(i)} \in \mathbb{R}^M$, the scLLM produces a contextualized embedding $\mathbf{h}_{\text{cell}} = \text{scGPT}(\widetilde{\mathbf{x}}^{(i)})$. This is passed through a Q-former to yield the cell feature $\mathbf{c} = \text{QFormer}(\mathbf{h}_{\text{cell}})$. Similarly, for a textual description represented by the token sequence $\mathbf{t}^{(\mathbf{i})} = \{t_1, \ldots, t_L\}$, we extract the text embedding via the BERT module within the Q-Former as $\mathbf{h}_{text} = \text{BERT}(\mathbf{t}^{(i)})$.

During this stage, parameters of both the cell encoder and Q-Former are updated. We compute the alignment loss as a combination of the cell-text contrastive InfoNCE loss $\mathcal{L}_{\text{InfoNCE}}$ (Chen et al., 2020), and a cross-entropy cell-text matching loss $\mathcal{L}_{\text{CE}}$ (Li et al., 2023), thereby bringing paired representations closer while pushing unpaired ones apart:

$$\mathcal{L}_{\text{align}} = \mathcal{L}_{\text{InfoNCE}}(\mathbf{c}, \mathbf{t}) + \mathcal{L}_{\text{CE}}(\mathbf{c}, \mathbf{t}). \tag{2}$$

Contrastive Cell Representation Learning. In Stage 1, we perform joint contrastive learning along with the cross-modal discriminative pre-training for improved cell representation. Specifically, single-cell gene expression profiles are inherently noisy, suffering from high sparsity, dropout events, and technical variations caused by sequencing depth limits. Consequently, cells sharing the same biological state may exhibit significantly different raw expression values. To mitigate this issue and learn robust cell representations, we introduce a contrastive objective that leverages the intrinsic invariance of scRNA-seq data. For cell profile $\mathbf{x}$, we generate two correlated views, $\mathbf{v}_1$ and $\mathbf{v}_2$, by applying a stochastic augmentation pipeline designed to simulate scRNA-seq technical artifacts:

- **Random Masking:** A random fraction of expressed genes are set to zero. This encourages the model to recover cell identity even when partial gene information is missing, mimicking the zero-inflation characteristic of scRNA-seq data.
- **Gaussian Jitter:** Multiplicative Gaussian noise is injected into non-zero gene values: $x_j \leftarrow x_j \cdot (1 + \epsilon)$, where $\epsilon \sim \mathcal{N}(0, \sigma^2)$. This ensures the representation is robust to small fluctuations in expression counts.

To align these views, we employ a contrastive objective that maximizes the agreement between latent representations of the same cell while distinguishing them from different cells in the batch. By treating augmented views of the same cell as positive pairs and all others as negatives, the objective forces the encoder to learn features invariant to stochastic perturbations. This process effectively filters out technical artifacts—such as dropout noise—and focuses the model on intrinsic biological signals. The resulting regularization yields a compact and robust latent manifold, providing a stable foundation for subsequent cross-modal integration.

Stage 2: Cross-modal generative pre-training. We further pre-train the model with cross-modal generative objectives to enhance the bidirectional knowledge injection:

- **Cell → Text Generation:** Given a cell embedding processed by the cell encoder and projected via the cell-to-text module, we condition the decoder-only text LLM to autoregressively generate corresponding textual descriptions. The objective is defined as:

$$\mathcal{L}_{\text{c2t}} = -\sum_{l=1}^{L} \log p(t_l \mid t_{<l}, \mathbf{c}), \tag{3}$$

  where t_l denotes the l-th token of the generated text, and $\mathbf{c}$ represents the projected cell embedding.
- **Text → Cell Generation:** In the reverse direction, we enable the generation of cell embeddings conditioned on textual input. We first generate intermediate embedding with the text LLM: $\mathbf{c}' = \text{mlp}(\text{Llama}(t_{\leq L}))$. A lightweight text-to-cell projector then transforms this intermediate embedding into a soft prompt for the scLLM. The scLLM then predicts a pseudo-cell expression vector $\mathbf{x}' = \text{scGPT}(\mathbf{c}') \in \mathbb{R}^M$. We optimize the gene prediction head of scGPT with a mean squared error (MSE) loss:

$$\mathcal{L}_{\text{t2c}} = \sum_{1 \leq j \leq M} \text{MSE}(x'_j, \widetilde{x}_j), \tag{4}$$

  where $\widetilde{x}_j$ denotes the ground-truth normalized expression.

During this generative pre-training phase, we freeze the parameters of the cell-to-text projector and update the parameters of the text LLM, scLLM, and the text-to-cell projector by minimizing the combined loss $\mathcal{L}_{\text{c2t}} + \mathcal{L}_{\text{t2c}}$.

3.4 Adapting scMMGPT to Downstream Tasks

After two-stage pre-training, scMMGPT can be applied to various single-cell analysis tasks, either in a zero-shot manner or with additional fine-tuning.

Cell Type Annotation. We leverage scMMGPT's ability to discern similarities between scRNA-seq profiles and cell-type text descriptions. In the zero-shot scenario, we directly use the stage-2 pre-trained scLLM and Q-former for annotation. Given a cell $\mathbf{x}^{(i)}$, we calculate its contrastive and matching losses against textual descriptions $\{\mathbf{t}_j\}$ of all possible cell types, and select the class that minimizes the combined loss $\lambda\mathcal{L}_{\text{InfoNCE}} + (1 - \lambda)\mathcal{L}_{\text{CE}}$ as prediction. In the fine-tuning scenario, we continue training scMMGPT on the downstream dataset using the alignment loss $\mathcal{L}_{\text{align}}$, and employ the same inference approach as in the zero-shot case.

Batch Effect Correction and Cell Clustering. These tasks evaluate the quality of cell representations derived from the model. Specifically, we leverage the fully pre-trained scLLM (*i.e.,* scGPT) from

Table 1: Results of cell type annotation (%) with fine-tuning. Asterisk (*) denotes results borrowed from previous studies (Cui et al., 2024; Liu et al., 2023b). **Bold** denotes best results. Green highlights relative improvements.

Method	**Myeloid**		**hPancreas**		**Multiple Sclerosis**		**PBMC-3K**	
	Accuracy (%)	F1 (%)	Accuracy (%)	F1 (%)	Accuracy (%)	F1 (%)	Accuracy (%)	F1 (%)
scBERT (Yang et al., 2022)*	52.5	29.8	96.4	68.5	78.5	59.9	23.5	13.1
scGPT (Cui et al., 2024)*	64.2	34.6	96.8	71.8	85.6	70.3	93.3	80.7
Geneformer (Theodoris et al., 2023)	59.3	35.6	96.6	77.3	71.3	74.4	86.4	65.0
LangCell (Zhao et al., 2024)	58.9	35.7	96.3	70.8	72.9	71.2	90.6	81.2
scELMo (Liu et al., 2023b)*	-	-	96.8	68.0	-	-	90.3	83.5
scMMGPT	**69.0**$^{+7.48\%}$	**67.6**$^{+89.36\%}$	**98.2**$^{+1.45\%}$	**81.1**$^{+4.92\%}$	**87.4**$^{+2.10\%}$	**84.5**$^{+13.58\%}$	**94.8**$^{+4.64\%}$	**93.5**$^{+11.98\%}$

Table 2: Results of cell clustering on PBMC-10K (Gayoso et al., 2022) and COVID-19 (Lotfollahi et al., 2022b) datasets. Green highlights relative improvements.

Dataset	Model	Avg_{bio} (↑)	NMI_{cell} (↑)	ARI_{cell} (↑)	ASW_{cell} (↑)	$\text{Avg}_{\text{batch}}$ (↑)	$\text{ASW}_{\text{batch}}$ (↑)	$\text{Graph}_{\text{conn}}$ (↑)
PBMC-10K	Seurat	0.724	0.808	0.722	0.641	0.940	0.960	0.920
	Harmony	0.784	0.860	0.902	0.591	0.940	0.975	0.906
	scVI	0.753	0.819	0.847	0.592	0.947	0.967	0.928
	scGPT	0.821	0.850	0.873	0.740	0.923	0.950	0.895
	Geneformer	0.793	0.825	0.846	0.709	-	0.928	-
	LangCell	0.808	0.845	0.854	0.724	-	0.979	-
	scMMGPT	**0.854**$^{+4.02\%}$	**0.885**$^{+2.91\%}$	**0.928**$^{+3.00\%}$	**0.748**$^{+1.08\%}$	**0.988**$^{+4.33\%}$	**0.983**$^{+0.41\%}$	**0.993**$^{+7.00\%}$
COVID-19	Seurat	0.413	0.513	0.289	0.437	0.790	0.799	0.781
	Harmony	0.327	0.482	0.185	0.313	0.680	0.642	0.720
	scVI	0.502	0.638	0.408	0.461	0.838	0.833	0.844
	scGPT	0.504	0.659	0.400	0.452	0.850	0.826	0.874
	scMMGPT	**0.545**$^{+8.13\%}$	**0.668**$^{+1.37\%}$	**0.454**$^{+11.27\%}$	**0.512**$^{+11.06\%}$	**0.892**$^{+4.94\%}$	**0.875**$^{+5.04\%}$	**0.908**$^{+3.89\%}$

both stages for zero-shot cell feature extraction. Formally, given a set of cells $\{\mathbf{x}^{(i)}\}$, we obtain their representations as $\mathbf{c}^{(i)} = \text{scGPT}(\mathbf{x}^{(i)})$, which are then utilized for clustering.

Cell Description Generation. For cell description generation tasks, we further fine-tune the text LLM with the cell-to-text translation loss $\mathcal{L}_{\text{c2t}}$, while freezing both the scLLM and the Q-former. During inference, we autoregressively generate descriptions conditioned on the cell embedding $\mathbf{c}$.

4 Experiments

In experiment, we aim to answer these Research Questions (RQ):

RQ1: How effectively does scMMGPT enhance single-cell analysis tasks (cell type annotation, clustering, and text generation) by integrating biological priors from scRNA-seq and text?

RQ2: How do the discriminative and generative pre-training objectives synergistically contribute to the alignment and knowledge transfer between single-cell and text modalities?

RQ3: Does scMMGPT achieve robust generalization in challenging out-of-distribution scenarios?

Experiment Setup. scMMGPT is pre-trained in two stages: Stage 1 for representation alignment spans 5 epochs, while Stage 2 cross-modal generation runs for 1 epoch. Unless otherwise indicated, we apply LoRA (Hu et al., 2022) adapters for parameter-efficient fine-tuning of text LLM, whereas the cell encoder and projection modules are fully trained. Further details are provided in Appendix C.

4.1 Effectiveness for Single-Cell Analysis (RQ1)

Here we demonstrate the effectiveness of scMMGPT across four different tasks. The performance of the fifth tasks pseudocell generation can be found in Appendix D.2.

Cell Type Annotation. Cell type annotation is to evaluate a model's ability to accurately annotate cells based on their scRNA-seq profiles. We compare scMMGPT against several baselines: scBERT (Yang et al., 2022), scGPT (Cui et al., 2024), Geneformer (Theodoris et al., 2023), LangCell (Zhao et al., 2024), and scELMo (Liu et al., 2023b). Accuracy and macro F1 score (F1) are used as evaluation metrics. We conduct experiments on four datasets: Myeloid (Cheng et al., 2021), hPancreas (Chen et al., 2023), Multiple Sclerosis (Schirmer et al., 2019), and PBMC-3K (Zheng et al., 2017). All the models are fine-tuned on the downstream training dataset before the evaluation.

Table 3: Results of cell description generation on the immune tissue (Domínguez Conde et al., 2022) dataset.

Model	Accuracy (↑)	F1 (↑)	BLEU-2 (↑)	ROUGE-2 (↑)	METEOR (↑)	MMD (↓)	EMD (↓)
GPT-2 Small (Radford et al., 2019)	21.96%	12.58%	36.82%	26.49%	38.61%	0.189	0.020
GPT-2 Large (Radford et al., 2019)	33.93%	15.99%	41.31%	35.18%	44.02%	0.127	0.020
LLaMA2-7B-Instruct (Touvron et al., 2023b)	68.19%	56.93%	45.48%	69.80%	76.60%	0.097	0.014
C2S Small (Levine et al., 2024)	35.05%	25.67%	50.07%	47.53%	55.38%	0.043	0.016
C2S Large (Levine et al., 2024)	59.24%	54.97%	73.38%	68.54%	74.32%	0.020	0.009
scMMGPT	**87.56%**$^{+28.41\%}$	**86.93%**$^{+52.70\%}$	**91.45%**$^{+24.63\%}$	**92.55%**$^{+32.59\%}$	**90.72%**$^{+18.43\%}$	**0.010**$^{-49.8\%}$	**0.005**$^{-46.5\%}$

The experimental results are summarized in Table 1. Asterisk (*) denotes results borrowed from previous studies (Cui et al., 2024; Liu et al., 2023b). scMMGPT consistently outperforms existing methods across all evaluated datasets, achieving steady improvements in accuracy and up to about 10% increase in F1 scores (Multiple Sclerosis and PBMC-3K). These results validate scMMGPT's superior classification performance and its strong adaptability across different biological contexts and tissue distributions.

Cell Clustering. Cell clustering plays a fundamental role in novel cell type discovery and helps remove the batch effects in scRNA-seq data, which are introduced by different experiment batches. We evaluate scMMGPT on cell clustering tasks using the PBMC-10K (Gayoso et al., 2022) and COVID-19 (Lotfollahi et al., 2022b) datasets, comparing it against several scLLMs and softwares: Seurat (Satija et al., 2015), Harmony (Korsunsky et al., 2019), scVI (Lopez et al., 2018), scGPT (Cui et al., 2024), Geneformer (Theodoris et al., 2023), and LangCell (Zhao et al., 2024). We use standard biological conservation (NMI$_{cell}$, ARI$_{cell}$, and ASW$_{cell}$) and batch correction (ASW$_{batch}$ and Graph$_{Conn}$) metrics (Luecken et al., 2022) to assess performance, which can be summarized into Avg$_{\text{bio}}$ and Avg$_{\text{batch}}$ scores. The detailed explanations of these metrics are in Appendix C.3.

As shown in Table 2, scMMGPT consistently outperforms all baselines across both biological conservation and batch correction metrics. On both datasets, scMMGPT achieves an Avg$_{\text{bio}}$ improvement of 4% and 8%, and an Avg$_{\text{batch}}$ improvement of at least 4%. These results highlight its strong ability to preserve biological structure while effectively correcting batch effects.

Cell Description Generation. Cell description generation is to produce cells' textual descriptions using scRNA-seq data. We compare against GPT-2 (Radford et al., 2019) and C2S (Levine et al., 2024) on the immune tissue (Domínguez Conde et al., 2022) dataset. We use Maximum Mean Discrepancy (MMD) and Earth Mover's Distance (EMD) to measure semantic similarity based on text embeddings (Xiao et al., 2024), alongside BLEU (Papineni et al., 2002), ROUGE (Lin, 2004), and METEOR (Banerjee & Lavie, 2005) to measure rule-based text similarity. We also measure the cell annotation accuracy and F1 scores based on the cell type text extracted from the cell descriptions.

As shown in Table 3, scMMGPT substantially outperforms prior baselines, achieving higher text similarity and semantic alignment with ground-truth descriptions. It improves classification metrics by nearly 30%, rule-based text similarities by about 20%, and reduces MMD and EMD by nearly 50%. These results indicate the strong biological relevance of the descriptions generated by scMMGPT.

Perturbation Prediction. We evaluate the perturbation prediction capability by predicting the post-perturbation gene expression profile given an input control cell state and the perturbed gene(s). Following the setting of scGPT (Cui et al., 2024), we fine-tune each model on a subset of perturbations and test it on perturbations involving unseen genes. We report Pearson$_\delta$, which measures the correlation between predicted and observed expression changes after perturbation. We further report Pearson$_\delta$+de, computed on the top-20 differentially expressed genes for each perturbation. As Table 4 shows, scMMGPT consistently outperforms scGPT, GEARS (Roohani et al., 2024), and the linear regression (LR) baseline for both datasets.

Table 4: Results of perturbation prediction on Adamson and Norman datasets. Higher is better.

Dataset	Model	Pearson$_\delta$ (↑)	Pearson$_\delta$+de (↑)
Adamson	**scMMGPT**	**0.633**$^{+2.93\%}$	**0.791**$^{+0.25\%}$
	scGPT	0.615	0.789
	GEARS	0.531	0.678
	LR	0.387	0.620
Norman	**scMMGPT**	**0.587**$^{+0.69\%}$	**0.752**$^{+1.35\%}$
	scGPT	0.583	0.742
	GEARS	0.547	0.715
	LR	0.387	0.620

Table 5: Ablation studies of cell type annotation on various datasets.

Method	Myeloid		hPancreas		Multiple Sclerosis		PBMC-3K	
	Accuracy	F1	Accuracy	F1	Accuracy	F1	Accuracy	F1
scMMGPT	**68.96**	**67.57**	**98.22**	**81.06**	87.38	**84.49**	**94.83**	**93.51**
Ablation over Training Stages								
No Pre-train Stage 2	67.44	66.78	97.63	80.56	**87.79**	83.40	94.72	93.36
No Pre-train Stage 1&2	67.56	63.22	77.13	44.03	84.98	76.45	94.72	91.41
Stage 1 w/o $\mathcal{L}_{\text{InfoNCE}}$	64.21	64.43	93.62	68.94	86.41	81.22	94.50	93.17
Stage 1 w/o $\mathcal{L}_{\text{CE}}$	68.26	63.06	96.70	74.52	86.82	82.77	94.61	92.04
scLLM from scratch	66.13	64.11	97.18	81.40	75.94	75.72	92.36	82.52
Ablation over generative objectives								
Stage2 w/o c2t	67.42	67.15	96.92	79.96	86.55	83.69	94.29	92.86
Stage2 w/o t2c	67.74	66.74	97.11	79.93	87.32	82.75	94.50	93.14
Ablation over Cross-model Projector								
use MLP instead of Qformer	66.60	64.51	96.73	74.41	86.23	83.38	94.72	91.92
Ablation over Text Source								
only cell metadata	67.97	67.54	97.79	80.76	87.51	82.15	94.18	91.39
only free text	67.94	66.69	96.56	74.41	83.03	78.23	94.83	93.34

Table 6: Results of cell type annotation (%) on the Tabula Sapiens (Consortium* et al., 2022) dataset. The models are fine-tuned on a certain proportion of test cell types. Acc@N denotes top-N accuracy. Green highlights relative improvements.

	Zero-Shot			Fine-tuned on 10% Types			Fine-tuned on 20% Types			Fine-tuned on 30% Types		
Model	Acc@1	Acc@5	Acc@10	Acc@1	Acc@5	Acc@10	Acc@1	Acc@5	Acc@10	Acc@1	Acc@5	Acc@10
Random	0.6	3.1	6.2	0.6	3.1	6.2	0.6	3.1	6.2	0.6	3.1	6.2
BioTranlator	-	-	-	3.5	33.6	45.4	13.4	48.2	63.5	13.7	50.6	68.6
LangCell	28.6	69.2	82.9	30.5	71.0	83.7	35.0	74.6	86.4	38.2	83.0	92.1
scMMGPT	**49.1**$^{+71.7\%}$	**83.1**$^{+19.9\%}$	**91.1**$^{+9.9\%}$	**55.7**$^{+82.6\%}$	**89.2**$^{+25.6\%}$	**96.0**$^{+14.7\%}$	**59.7**$^{+71.1\%}$	**90.4**$^{+21.2\%}$	**96.8**$^{+12.0\%}$	**60.9**$^{+59.4\%}$	**93.6**$^{+12.8\%}$	**98.4**$^{+7.0\%}$

4.2 Ablation Studies (RQ2)

We conduct systematic ablation studies to evaluate the effectiveness of each key component.

Impact of Training Stages. We first assess the effectiveness of our multi-stage training process. We compare five different pre-training variations: (1) using the full pre-training pipeline, (2) using a randomly initialized scLLM instead of a pre-trained one, (3) removing $\mathcal{L}_{\text{InfoNCE}}$ or $\mathcal{L}_{\text{CE}}$ loss in stage 1 pre-training, (4) removing stage 2 pre-training, and (5) removing both stage 1&2 pre-training. As shown in Table 5, the full training pipeline yields the best results, with clear improvements in both accuracy and F1-score.

Impact of Text Source. We next investigate how different textual inputs affect performance. We evaluate three variations: (1) using both cell metadata and free-text descriptions as the text source, (2) using metadata only, and (3) using free-text only. As shown in Table 5, combining metadata and free-text leads to the highest accuracy and F1-score. This highlights that structured and unstructured textual information provides complementary benefits.

Impact of Generative Objectives. We further study the role of the two generative objectives in stage 2 pre-training. Specifically, we ablate (1) cell-to-text generation (Stage2 w/o c2t) and (2) text-to-cell generation (Stage2 w/o t2c). As Table 5 shows, both objectives contribute to cross-modal alignment.

Impact of Model Architecture. We examine the effect of the Q-former in capturing cross-modal interactions. We try an MLP variant of scMMGPT where the Q-former projector is replaced with simple MLP layers while keeping other components unchanged. As shown in Table 5, the original Q-former design outperforms the MLP variant across all metrics, highlighting its effectiveness in modeling fine-grained relationships between modalities.

4.3 Out-of-Distribution Evaluation (RQ3)

We evaluate the model's cell annotation performance under out-of-distribution settings. The experiment is conducted on the Tabula Sapiens (Consortium* et al., 2022) dataset, which comprises 161 distinct human cell types, most absent from our pre-training corpus. We report the accuracies under fine-tuning settings, where the model is trained on different proportions of test cell types (10%, 20%, and 30%) and tested on the remaining proportions. We compare our model against two baseline methods, BioTranslator (Xu et al., 2023a) and LangCell (Zhao et al., 2024). Top-N accuracies (Acc@N) are used as the metric.

Experimental results are shown in Table 6. scMMGPT achieves an Acc@1 of 49.1% and an Acc@5 of 83.1% without further fine-tuning, surpassing certain fine-tuned baselines. As the proportion of fine-tuning cell types increases, scMMGPT consistently improves its performance across all metrics, reaching a maximum Acc@1 of 60.9% when fine-tuned on 30% cell types. These results demonstrate that scMMGPT's pre-trained knowledge of cellular and textual data enables strong generalization to unseen cell types.

5 Conclusion and Future Works

In this study, we introduce scMMGPT, a multimodal foundation model for comprehensive single-cell analysis. By effectively bridging scRNA-seq data with textual information, scMMGPT supports a range of tasks, including cell type annotation, cell clustering, perturbation prediction, cell description generation, and pseudo cell generation. This multi-modal integration is achieved through the synergistic use of an scLLM and a text PLM, connected by our innovative cross-modal pretraining. Trained on 27 million cells from the CELLxGENE dataset, scMMGPT demonstrates superior performance across diverse single-cell analysis applications.

Looking forward, we aim to expand scMMGPT by incorporating datasets of more species and integrating more cell modalities, including scATAC-seq and CITE-seq. This expansion will empower scMMGPT to address more challenges of multi-omic integration (Lotfollahi et al., 2022a), cross-omic translation (Liu et al., 2023a), and novel cell type discovery (Yang et al., 2022), significantly enhancing its utility in single-cell research.

References

Jean-Baptiste Alayrac, Jeff Donahue, Pauline Luc, Antoine Miech, Iain Barr, Yana Hasson, Karel Lenc, Arthur Mensch, Katherine Millican, Malcolm Reynolds, et al. Flamingo: a visual language model for few-shot learning. *Advances in neural information processing systems*, 35:23716–23736, 2022.

Philipp Angerer, Lukas Simon, Sophie Tritschler, F Alexander Wolf, David Fischer, and Fabian J Theis. Single cells make big data: new challenges and opportunities in transcriptomics. *Current opinion in systems biology*, 4:85–91, 2017.

Satanjeev Banerjee and Alon Lavie. Meteor: An automatic metric for mt evaluation with improved correlation with human judgments. In *Proceedings of the acl workshop on intrinsic and extrinsic evaluation measures for machine translation and/or summarization*, pp. 65–72, 2005.

Haiyang Bian, Yixin Chen, Xiaomin Dong, Chen Li, Minsheng Hao, Sijie Chen, Jinyi Hu, Maosong Sun, Lei Wei, and Xuegong Zhang. scmulan: a multitask generative pre-trained language model for single-cell analysis. In *International Conference on Research in Computational Molecular Biology*, pp. 479–482, 2024.

Kathi Canese and Sarah Weis. Pubmed: the bibliographic database. *The NCBI handbook*, 2(1), 2013.

He Cao, Zijing Liu, Xingyu Lu, Yuan Yao, and Yu Li. Instructmol: Multi-modal integration for building a versatile and reliable molecular assistant in drug discovery. In Owen Rambow, Leo Wanner, Marianna Apidianaki, Hend Al-Khalifa, Barbara Di Eugenio, and Steven Schockaert (eds.), *Proceedings of the 31st International Conference on Computational Linguistics, COLING 2025, Abu Dhabi, UAE, January 19-24, 2025*, pp. 354–379, 2025.

Zhi-Jie Cao and Ge Gao. Multi-omics single-cell data integration and regulatory inference with graph-linked embedding. *Nature Biotechnology*, 40(10):1458–1466, 2022.

Jiawei Chen, Hao Xu, Wanyu Tao, Zhaoxiong Chen, Yuxuan Zhao, and Jing-Dong J. Han. Transformer for one stop interpretable cell type annotation. *Nature Communications*, 14(1):223, January 2023. ISSN 2041-1723. doi: 10.1038/s41467-023-35923-4.

Ting Chen, Simon Kornblith, Mohammad Norouzi, and Geoffrey Hinton. A simple framework for contrastive learning of visual representations, 2020. URL https://arxiv.org/abs/2002.05709.

Yiqun Chen and James Zou. Genept: a simple but effective foundation model for genes and cells built from chatgpt. *bioRxiv*, pp. 2023–10, 2023.

Sijin Cheng, Ziyi Li, Ranran Gao, Baocai Xing, Yunong Gao, Yu Yang, Shishang Qin, Lei Zhang, Hanqiang Ouyang, Peng Du, et al. A pan-cancer single-cell transcriptional atlas of tumor infiltrating myeloid cells. *Cell*, 184(3):792–809, 2021.

Hongyoon Choi, Jeongbin Park, Sumin Kim, Jiwon Kim, Dongjoo Lee, Sungwoo Bae, Haenara Shin, and Daeseung Lee. Cellama: Foundation model for single cell and spatial transcriptomics by cell embedding leveraging language model abilities. *bioRxiv*, pp. 2024–05, 2024.

The Tabula Sapiens Consortium*, Robert C Jones, Jim Karkanias, Mark A Krasnow, Angela Oliveira Pisco, Stephen R Quake, Julia Salzman, Nir Yosef, Bryan Bulthaup, Phillip Brown, et al. The tabula sapiens: A multiple-organ, single-cell transcriptomic atlas of humans. *Science*, 376(6594): eabl4896, 2022.

Haotian Cui, Chloe Wang, Hassaan Maan, Kuan Pang, Fengning Luo, Nan Duan, and Bo Wang. scgpt: toward building a foundation model for single-cell multi-omics using generative ai. *Nature Methods*, pp. 1–11, 2024.

C Domínguez Conde, C Xu, LB Jarvis, DB Rainbow, SB Wells, T Gomes, SK Howlett, O Suchanek, K Polanski, HW King, et al. Cross-tissue immune cell analysis reveals tissue-specific features in humans. *Science*, 376(6594):eabl5197, 2022.

Carl Edwards, Tuan Manh Lai, Kevin Ros, Garrett Honke, Kyunghyun Cho, and Heng Ji. Translation between molecules and natural language. In *Proceedings of the 2022 Conference on Empirical Methods in Natural Language Processing, EMNLP 2022, Abu Dhabi, United Arab Emirates, December 7-11, 2022*, pp. 375–413, 2022.

Junfeng Fang, Shuai Zhang, Chang Wu, Zhengyi Yang, Zhiyuan Liu, Sihang Li, Kun Wang, Wenjie Du, and Xiang Wang. Moltc: Towards molecular relational modeling in language models. *arXiv preprint arXiv:2402.03781*, 2024.

Yin Fang, Xinle Deng, Kangwei Liu, Ningyu Zhang, Jingyang Qian, Penghui Yang, Xiaohui Fan, and Huajun Chen. A multi-modal ai copilot for single-cell analysis with instruction following. *arXiv preprint arXiv:2501.08187*, 2025.

Oscar Franzén, Li-Ming Gan, and Johan LM Björkegren. Panglaodb: a web server for exploration of mouse and human single-cell rna sequencing data. *Database*, 2019:baz046, 2019.

Adam Gayoso, Romain Lopez, Galen Xing, Pierre Boyeau, Valeh Valiollah Pour Amiri, Justin Hong, Katherine Wu, Michael Jayasuriya, Edouard Mehlman, Maxime Langevin, et al. A python library for probabilistic analysis of single-cell omics data. *Nature biotechnology*, 40(2):163–166, 2022.

Yu Gu, Robert Tinn, Hao Cheng, Michael Lucas, Naoto Usuyama, Xiaodong Liu, Tristan Naumann, Jianfeng Gao, and Hoifung Poon. Domain-specific language model pretraining for biomedical natural language processing. *ACM Transactions on Computing for Healthcare (HEALTH)*, 3(1): 1–23, 2021.

Minsheng Hao, Jing Gong, Xin Zeng, Chiming Liu, Yucheng Guo, Xingyi Cheng, Taifeng Wang, Jianzhu Ma, Xuegong Zhang, and Le Song. Large-scale foundation model on single-cell transcriptomics. *Nature Methods*, pp. 1–11, 2024.

Lukas Heumos, Anna C Schaar, Christopher Lance, Anastasia Litinetskaya, Felix Drost, Luke Zappia, Malte D Lücken, Daniel C Strobl, Juan Henao, Fabiola Curion, et al. Best practices for single-cell analysis across modalities. *Nature Reviews Genetics*, 24(8):550–572, 2023.

Edward J. Hu, Yelong Shen, Phillip Wallis, Zeyuan Allen-Zhu, Yuanzhi Li, Shean Wang, Lu Wang, and Weizhu Chen. Lora: Low-rank adaptation of large language models. In *The Tenth International Conference on Learning Representations, ICLR 2022, Virtual Event, April 25-29, 2022*, 2022.

Yuge Ji, Mohammad Lotfollahi, F Alexander Wolf, and Fabian J Theis. Machine learning for perturbational single-cell omics. *Cell Systems*, 12(6):522–537, 2021.

Ilya Korsunsky, Nghia Millard, Jean Fan, Kamil Slowikowski, Fan Zhang, Kevin Wei, Yuriy Baglaenko, Michael Brenner, Po-ru Loh, and Soumya Raychaudhuri. Fast, sensitive and accurate integration of single-cell data with harmony. *Nature methods*, 16(12):1289–1296, 2019.

Daniel Levine, Syed A Rizvi, Sacha Lévy, Nazreen Pallikkavaliyaveetil, David Zhang, Xingyu Chen, Sina Ghadermarzi, Ruiming Wu, Zihe Zheng, Ivan Vrkic, et al. Cell2sentence: Teaching large language models the language of biology. In *Forty-first International Conference on Machine Learning*, 2024.

Junnan Li, Dongxu Li, Silvio Savarese, and Steven Hoi. Blip-2: Bootstrapping language-image pre-training with frozen image encoders and large language models. In *International conference on machine learning*, pp. 19730–19742, 2023.

Sihang Li, Zhiyuan Liu, Yanchen Luo, Xiang Wang, Xiangnan He, Kenji Kawaguchi, Tat-Seng Chua, and Qi Tian. 3d-molm: Towards 3d molecule-text interpretation in language models. In *ICLR*, 2024.

Xiang Lisa Li and Percy Liang. Prefix-tuning: Optimizing continuous prompts for generation. In *ACL/IJCNLP (1)*, pp. 4582–4597. Association for Computational Linguistics, 2021.

Chin-Yew Lin. Rouge: A package for automatic evaluation of summaries. In *Text summarization branches out*, pp. 74–81, 2004.

Yingxin Lin, Tung-Yu Wu, Sheng Wan, Jean YH Yang, Wing H Wong, and YX Rachel Wang. scjoint integrates atlas-scale single-cell rna-seq and atac-seq data with transfer learning. *Nature biotechnology*, 40(5):703–710, 2022.

Linjing Liu, Wei Li, Ka-Chun Wong, Fan Yang, and Jianhua Yao. A pre-trained large generative model for translating single-cell transcriptome to proteome. *bioRxiv*, pp. 2023–07, 2023a.

Tianyu Liu, Tianqi Chen, Wangjie Zheng, Xiao Luo, and Hongyu Zhao. scelmo: Embeddings from language models are good learners for single-cell data analysis. *bioRxiv*, pp. 2023–12, 2023b.

Zhiyuan Liu, Sihang Li, Yanchen Luo, Hao Fei, Yixin Cao, Kenji Kawaguchi, Xiang Wang, and Tat-Seng Chua. Molca: Molecular graph-language modeling with cross-modal projector and uni-modal adapter. In *Proceedings of the 2023 Conference on Empirical Methods in Natural Language Processing, EMNLP 2023, Singapore, December 6-10, 2023*, pp. 15623–15638, 2023c.

Zhiyuan Liu, Yaorui Shi, An Zhang, Enzhi Zhang, Kenji Kawaguchi, Xiang Wang, and Tat-Seng Chua. Rethinking tokenizer and decoder in masked graph modeling for molecules. In *NeurIPS*, 2023d.

Zhiyuan Liu, Yaorui Shi, An Zhang, Sihang Li, Enzhi Zhang, Xiang Wang, Kenji Kawaguchi, and Tat-Seng Chua. Reactxt: Understanding molecular ”reaction-ship” via reaction-contextualized molecule-text pretraining. In Lun-Wei Ku, Andre Martins, and Vivek Srikumar (eds.), *Findings of the Association for Computational Linguistics, ACL 2024, Bangkok, Thailand and virtual meeting, August 11-16, 2024*, pp. 5353–5377, 2024a.

Zhiyuan Liu, An Zhang, Hao Fei, Enzhi Zhang, Xiang Wang, Kenji Kawaguchi, and Tat-Seng Chua. Prott3: Protein-to-text generation for text-based protein understanding. In *ACL (1)*, pp. 5949–5966. Association for Computational Linguistics, 2024b.

Zhiyuan Liu, Yanchen Luo, Han Huang, Enzhi Zhang, Sihang Li, Junfeng Fang, Yaorui Shi, Xiang Wang, Kenji Kawaguchi, and Tat-Seng Chua. NEXT-MOL: 3d diffusion meets 1d language modeling for 3d molecule generation. In *The Thirteenth International Conference on Learning Representations*, 2025.

Romain Lopez, Jeffrey Regier, Michael B Cole, Michael I Jordan, and Nir Yosef. Deep generative modeling for single-cell transcriptomics. *Nature methods*, 15(12):1053–1058, 2018.

Mohammad Lotfollahi, F Alexander Wolf, and Fabian J Theis. scgen predicts single-cell perturbation responses. *Nature methods*, 16(8):715–721, 2019.

Mohammad Lotfollahi, Anastasia Litinetskaya, and Fabian J Theis. Multigrate: single-cell multi-omic data integration. *BioRxiv*, pp. 2022–03, 2022a.

Mohammad Lotfollahi, Mohsen Naghipourfar, Malte D Luecken, Matin Khajavi, Maren Büttner, Marco Wagenstetter, Žiga Avsec, Adam Gayoso, Nir Yosef, Marta Interlandi, et al. Mapping single-cell data to reference atlases by transfer learning. *Nature biotechnology*, 40(1):121–130, 2022b.

Malte D Luecken, Maren Büttner, Kridsadakorn Chaichoompu, Anna Danese, Marta Interlandi, Michaela F Müller, Daniel C Strobl, Luke Zappia, Martin Dugas, Maria Colomé-Tatché, et al. Benchmarking atlas-level data integration in single-cell genomics. *Nature methods*, 19(1):41–50, 2022.

Erpai Luo, Minsheng Hao, Lei Wei, and Xuegong Zhang. scdiffusion: conditional generation of high-quality single-cell data using diffusion model. *Bioinformatics*, 40(9):btae518, 2024a.

Yanchen Luo, Junfeng Fang, Sihang Li, Zhiyuan Liu, Jiancan Wu, An Zhang, Wenjie Du, and Xiang Wang. Text-guided small molecule generation via diffusion model. *iScience*, 27(11), 2024b.

Yuren Mao, Yu Mi, Peigen Liu, Mengfei Zhang, Hanqing Liu, and Yunjun Gao. scagent: Universal single-cell annotation via a llm agent. *arXiv preprint arXiv:2504.04698*, 2025.

Aaron van den Oord, Yazhe Li, and Oriol Vinyals. Representation learning with contrastive predictive coding. *arXiv preprint arXiv:1807.03748*, 2018.

OpenAI. Gpt-4 technical report. *arXiv preprint arXiv:2303.08774*, 2023.

Kishore Papineni, Salim Roukos, Todd Ward, and Wei-Jing Zhu. Bleu: a method for automatic evaluation of machine translation. In *Proceedings of the 40th annual meeting of the Association for Computational Linguistics*, pp. 311–318, 2002.

CZI Cell Science Program, Shibla Abdulla, Brian Aevermann, Pedro Assis, Seve Badajoz, Sidney M Bell, Emanuele Bezzi, Batuhan Cakir, Jim Chaffer, Signe Chambers, et al. Cz cellxgene discover: a single-cell data platform for scalable exploration, analysis and modeling of aggregated data. *Nucleic Acids Research*, 53(D1):D886–D900, 2025.

Alec Radford, Jeffrey Wu, Rewon Child, David Luan, Dario Amodei, Ilya Sutskever, et al. Language models are unsupervised multitask learners. *OpenAI blog*, 1(8):9, 2019.

Yusuf Roohani, Kexin Huang, and Jure Leskovec. Predicting transcriptional outcomes of novel multigene perturbations with gears. *Nature Biotechnology*, 42(6):927–935, 2024.

Antoine-Emmanuel Saliba, Alexander J Westermann, Stanislaw A Gorski, and Jörg Vogel. Single-cell rna-seq: advances and future challenges. *Nucleic acids research*, 42(14):8845–8860, 2014.

Rahul Satija, Jeffrey A Farrell, David Gennert, Alexander F Schier, and Aviv Regev. Spatial reconstruction of single-cell gene expression data. *Nature biotechnology*, 33(5):495–502, 2015.

Moritz Schaefer, Peter Peneder, Daniel Malzl, Mihaela Peycheva, Jake Burton, Anna Hakobyan, Varun Sharma, Thomas Krausgruber, Joerg Menche, Eleni M Tomazou, et al. Multimodal learning of transcriptomes and text enables interactive single-cell rna-seq data exploration with natural-language chats. *bioRxiv*, pp. 2024–10, 2024.

Lucas Schirmer, Dmitry Velmeshev, Staffan Holmqvist, Max Kaufmann, Sebastian Werneburg, Diane Jung, Stephanie Vistnes, John H Stockley, Adam Young, Maike Steindel, et al. Neuronal vulnerability and multilineage diversity in multiple sclerosis. *Nature*, 573(7772):75–82, 2019.

Alex K Shalek, Rahul Satija, Joe Shuga, John J Trombetta, Dave Gennert, Diana Lu, Peilin Chen, Rona S Gertner, Jellert T Gaublomme, Nir Yosef, et al. Single-cell rna-seq reveals dynamic paracrine control of cellular variation. *Nature*, 510(7505):363–369, 2014.

Adam D Silverman, Ashty S Karim, and Michael C Jewett. Cell-free gene expression: an expanded repertoire of applications. *Nature Reviews Genetics*, 21(3):151–170, 2020.

Barry Smith, Michael Ashburner, Cornelius Rosse, Jonathan Bard, William Bug, Werner Ceusters, Louis J Goldberg, Karen Eilbeck, Amelia Ireland, Christopher J Mungall, et al. The obo foundry: coordinated evolution of ontologies to support biomedical data integration. *Nature biotechnology*, 25(11):1251–1255, 2007.

Christina V Theodoris, Ling Xiao, Anant Chopra, Mark D Chaffin, Zeina R Al Sayed, Matthew C Hill, Helene Mantineo, Elizabeth M Brydon, Zexian Zeng, X Shirley Liu, et al. Transfer learning enables predictions in network biology. *Nature*, 618(7965):616–624, 2023.

Hugo Touvron, Thibaut Lavril, Gautier Izacard, Xavier Martinet, Marie-Anne Lachaux, Timothée Lacroix, Baptiste Rozière, Naman Goyal, Eric Hambro, Faisal Azhar, et al. Llama: Open and efficient foundation language models. *arXiv preprint arXiv:2302.13971*, 2023a.

Hugo Touvron, Louis Martin, Kevin Stone, Peter Albert, Amjad Almahairi, Yasmine Babaei, Nikolay Bashlykov, Soumya Batra, Prajjwal Bhargava, Shruti Bhosale, et al. Llama 2: Open foundation and fine-tuned chat models. *arXiv preprint arXiv:2307.09288*, 2023b.

Ashish Vaswani, Noam Shazeer, Niki Parmar, Jakob Uszkoreit, Llion Jones, Aidan N Gomez, Łukasz Kaiser, and Illia Polosukhin. Attention is all you need. *Advances in neural information processing systems*, 30, 2017.

Chloe Wang, Haotian Cui, Andrew Zhang, Ronald Xie, Hani Goodarzi, and Bo Wang. scgpt-spatial: Continual pretraining of single-cell foundation model for spatial transcriptomics. *bioRxiv*, pp. 2025–02, 2025.

Hongzhi Wen, Wenzhuo Tang, Xinnan Dai, Jiayuan Ding, Wei Jin, Yuying Xie, and Jiliang Tang. Cellplm: Pre-training of cell language model beyond single cells. In *The Twelfth International Conference on Learning Representations*, 2023a.

Hongzhi Wen, Wenzhuo Tang, Wei Jin, Jiayuan Ding, Renming Liu, Xinnan Dai, Feng Shi, Lulu Shang, Hui Liu, and Yuying Xie. Single cells are spatial tokens: Transformers for spatial transcriptomic data imputation. *arXiv preprint arXiv:2302.03038*, 2023b.

Shitao Xiao, Zheng Liu, Peitian Zhang, Niklas Muennighoff, Defu Lian, and Jian-Yun Nie. C-pack: Packed resources for general chinese embeddings. In *Proceedings of the 47th international ACM SIGIR conference on research and development in information retrieval*, pp. 641–649, 2024.

Hanwen Xu, Addie Woicik, Hoifung Poon, Russ B Altman, and Sheng Wang. Multilingual translation for zero-shot biomedical classification using biotranslator. *Nature Communications*, 14(1):738, 2023a.

Minghao Xu, Xinyu Yuan, Santiago Miret, and Jian Tang. Protst: Multi-modality learning of protein sequences and biomedical texts. In *International Conference on Machine Learning*, pp. 38749–38767, 2023b.

Fan Yang, Wenchuan Wang, Fang Wang, Yuan Fang, Duyu Tang, Junzhou Huang, Hui Lu, and Jianhua Yao. scbert as a large-scale pretrained deep language model for cell type annotation of single-cell rna-seq data. *Nat. Mac. Intell.*, 4(10):852–866, 2022.

Duzhen Zhang, Yahan Yu, Jiahua Dong, Chenxing Li, Dan Su, Chenhui Chu, and Dong Yu. Mm-llms: Recent advances in multimodal large language models. *arXiv preprint arXiv:2401.13601*, 2024.

Suyuan Zhao, Jiahuan Zhang, and Zaiqing Nie. Large-scale cell representation learning via divide-and-conquer contrastive learning. *arXiv preprint arXiv:2306.04371*, 2023.

Suyuan Zhao, Jiahuan Zhang, Yushuai Wu, Yizhen Luo, and Zaiqing Nie. Langcell: Language-cell pre-training for cell identity understanding. In *Forty-first International Conference on Machine Learning*, 2024.

Grace X. Y. Zheng, Jessica M. Terry, Phillip Belgrader, Paul Ryvkin, Zachary W. Bent, Ryan Wilson, Solongo B. Ziraldo, Tobias D. Wheeler, Geoff P. McDermott, Junjie Zhu, Mark T. Gregory, Joe Shuga, Luz Montesclaros, Jason G. Underwood, Donald A. Masquelier, Stefanie Y. Nishimura, Michael Schnall-Levin, Paul W. Wyatt, Christopher M. Hindson, Rajiv Bharadwaj, Alexander Wong, Kevin D. Ness, Lan W. Beppu, H. Joachim Deeg, Christopher McFarland, Keith R. Loeb, William J. Valente, Nolan G. Ericson, Emily A. Stevens, Jerald P. Radich, Tarjei S. Mikkelsen, Benjamin J. Hindson, and Jason H. Bielas. Massively parallel digital transcriptional profiling of single cells. *Nature Communications*, 8(1):14049, January 2017. ISSN 2041-1723. doi: 10.1038/ncomms14049.

Christoph Ziegenhain, Beate Vieth, Swati Parekh, Björn Reinius, Amy Guillaumet-Adkins, Martha Smets, Heinrich Leonhardt, Holger Heyn, Ines Hellmann, and Wolfgang Enard. Comparative analysis of single-cell rna sequencing methods. *Molecular cell*, 65(4):631–643, 2017.

A Limitations and Ethical Considerations

Limited coverage of non-human species. A key limitation of scMMGPT is its reliance on pre-training data primarily sourced from the CELLxGENE dataset (Program et al., 2025), which focuses mainly on human tissues. This restricts the model's ability to generalize to cells from other species, such as those from widely used mouse datasets (Franzén et al., 2019).

Lack of incorporation of multiomics. Another major limitation is scMMGPT's exclusive focus on transcriptomic data, without incorporating other single-cell sequencing modalities such as scATAC-seq or CITE-seq (Liu et al., 2023a; Lin et al., 2022). By analyzing RNA abundance alone, the model misses critical insights into chromatin accessibility (scATAC-seq) and protein expression (CITE-seq). Integrating these modalities could provide a more comprehensive understanding of cellular states and regulatory mechanisms.

Exclusion of spatial transcriptomics. scMMGPT is restricted to analyzing individual cells, disregarding the spatial context. Spatially resolved transcriptomics captures gene expression and the physical organization of cells, thus revealing critical insights into cell-cell interactions and microenvironments (Wen et al., 2023b;a; Wang et al., 2025). Since scMMGPT operates solely on scRNA-seq data, it cannot leverage spatial relationships, which are often important in understanding tissue function and disease mechanisms.

Ethical considerations. Our pre-training and evaluation data are sourced from publicly available datasets, and we follow the original dataset licenses and usage terms; however, genomic data can still be sensitive, and users should ensure appropriate privacy protection, consent compliance, and access control when adapting the model to restricted-access or clinical data. The pre-training corpus is dominated by human tissues and a limited set of experimental protocols, which may introduce biases across populations, tissues, and sequencing platforms, and thus careful validation is recommended before deployment in underrepresented cohorts or new domains. Finally, while scMMGPT can accelerate biological analysis and drug discovery, it may be misused to support unsupported biomedical claims or downstream decisions without expert oversight; we emphasize that the model is intended for research use and should not be used as a standalone tool for clinical decision-making.

Table 7: Dataset statistics before and after data filtering.

Tissue/Category	Pre-filtering	Post-filtering
Brain	22 M	7.5 M
Lung	3.3 M	1.2 M
Pancreas	0.22 M	0.08 M
Pan-cancer	4.4 M	2.6 M
Kidney	1.0 M	0.35 M
Heart	2.2 M	0.7 M
Blood	5.4 M	4.2 M
Others	22 M	10.3 M
Total	60.5 M	26.9 M

B Details of Datasets

B.1 Collection of the Pre-training Dataset

B.1.1 Cell Transcriptomics Collection

The pre-training dataset for scMMGPT is constructed using publicly available data from the Cellx-Gene database (Program et al., 2025), with a snapshot taken on July 1, 2024. The dataset undergoes a series of filtering steps to ensure quality and consistency:

- We retain only human single-cell RNA sequencing (scRNA-seq) data, excluding entries from other species.

- We focus on data generated using the 10X Genomics platform, as its standardized outputs minimize technical variability across datasets.
- We deduplicate the dataset by keeping only one copy of each unique cell.
- To prevent information leakage, we remove all cells that appear in the test sets of downstream evaluation datasets.

After these filtering steps, the final dataset comprises approximately 27 million cells from 344 categories and 60697 different genes spanning diverse human tissues, including brain, lung, heart, blood, pancreas, kidney, pan-cancer, and others, as summarized in Figure 5. Table 7 shows the statistics of the dataset before and after the filtering.

B.1.2 Textual Description Collection

To ensure consistent and accurate cell-type annotations, we integrate standardized descriptions from two key resources: the Open Biomedical Ontologies Foundry (OBO Foundry) (Smith et al., 2007) and English Wikipedia. For each cell in the pre-training dataset, we first identify its biological classification (e.g., ”Tendon Cell”). These classifications are then mapped to formal definitions in OBO Foundry’s Cell Ontology, which provides machine-readable terms for cell types.

Additionally, we supplement these definitions with detailed explanations extracted from relevant Wikipedia entries, enriching the textual descriptions with accessible and comprehensive context.

Example Cell Description from Wikipedia.

Tendon Cell: Tendon cells, or tenocytes, are elongated fibroblast type cells. The cytoplasm is stretched between the collagen fibres of the tendon. They have a central cell nucleus with a prominent nucleolus. Tendon cells have a well-developed rough endoplasmic reticulum and they are responsible for synthesis and turnover of tendon fibres and ground substance.
Tendon cells form a connecting epithelial layer between the muscle and shell in molluscs. In gastropods, for example, the retractor muscles connect to the shell via tendon cells. Muscle cells are attached to the collagenous myo-tendon space via hemidesmosomes. The myo-tendon space is then attached to the base of the tendon cells via basal hemidesmosomes, while apical hemidesmosomes, which sit atop microvilli, attach the tendon cells to a thin layer of collagen. This is in turn attached to the shell via organic fibres which insert into the shell. Molluscan tendon cells appear columnar and contain a large basal cell nucleus. The cytoplasm is filled with granular endoplasmic reticulum and sparse golgi. Dense bundles of microfilaments run the length of the cell connecting the basal to the apical hemidesmosomes.

Example Cell Description from the Open Biomedical Ontologies Foundry.

Tendon Cell: An elongated fibrocyte that is part of a tendon. the cytoplasm is stretched between the collagen fibres of the tendon. they have a central cell nucleus with a prominent nucleolus. tendon cells have a well-developed rough endoplasmic reticulum and they are responsible for synthesis and turnover of tendon fibres and ground substance.

B.2 Collection of downstream Dataset

We collected multiple benchmark datasets to evaluate the performance of the scMMGPT model in various downstream tasks.

- **CellxGene (Program et al., 2025)**: CellxGene is an interactive data portal for single-cell transcriptomic data. It provides a graphical user interface for exploring and analyzing standardized single-cell datasets. The platform supports functions such as dataset discovery, download, analysis, and annotation. It has been used in machine learning to get millions of cells.
- **PBMC-10K (Gayoso et al., 2022)**: Integrating two independent scRNA-seq studies of healthy human peripheral blood mononuclear cells, this resource captures 3,346 actively expressed genes across 9 defined cell types: B cells, CD4+/CD8+ T lymphocytes, CD14+/FCGR3A+ monocytes, dendritic cells, natural killer cells, megakaryocytes, and rare

populations. The dataset serves as a standardized benchmark for methodological validation in immunogenomics.

- **Human Pancreas (Chen et al., 2023)**: The human pancreas (hPancreas) dataset includes data from five scRNA-seq studies of human pancreas cells and is divided into two parts. The reference set comes from two data sources, and the query set includes the other three. The dataset covers 3,000 genes. The reference set contains 10,600 cells across 13 cell types: alpha, beta, ductal, acinar, delta, pancreatic stellate, pancreatic polypeptide, endothelial, macrophage, mast, epsilon, Schwann, and T cells. The query set contains 4,218 cells across 11 cell types.

- **Multiple Sclerosis (Schirmer et al., 2019)**: This dataset includes nine healthy control samples and twelve MS samples, following the scGPT (Cui et al., 2024) setup. We use the control samples as the reference set for model fine-tuning and keep the MS samples as the query set for evaluation. The reference set contains 7,844 cells, and the query set contains 13,468 cells. The original publication provided cell type labels, which we use as the ground truth for evaluation. The dataset contains 18 cell types and covers 3,000 highly expressed genes.

- **Myeloid (Cheng et al., 2021)**: The myeloid dataset includes nine different cancer types. Six of them are used in the reference set for training, and the remaining three are used in the query set. The reference set includes the cancer types UCEC, PAAD, THCA, LYM, cDC2, and kidney. The query set includes MYE, OV-FTC, and ESCA. The reference set has 9,748 cells across 21 cell types. The query set has 3,430 cells across 11 cell types. The dataset covers 3,000 genes with high expression values.

- **PBMC-3K (Zheng et al., 2017)**: This dataset contains 4,638 cell samples. It includes eight types of cells: B cells, CD4+/CD8+ T lymphocytes, CD14+/FCGR3A+ monocytes, dendritic cells, natural killer cells, and megakaryocytes. The PBMC-3K dataset is characterized by the analysis of 14,236 unique genes. The dataset is made up of two different batches that represent separate experimental conditions.

- **Immune Tissue (Domínguez Conde et al., 2022)**: This comprehensive reference dataset profiles 360,000 human immune cells through single-cell RNA sequencing (scRNA-seq), systematically annotated with 35 distinct cell subtypes. Derived from 16 tissue types across 12 adult donors, it provides a cross-tissue characterization of lymphocyte, myeloid, and stromal cell populations, establishing a baseline for immunological studies.

- **Tabula Sapiens (Consortium* et al., 2022)**: Spanning 24 human organs with 483,152 single-cell profiles, this pan-tissue atlas identifies 161 rigorously validated cell types across epithelial, immune, endothelial, and stromal lineages. Incorporating demographic diversity through multi-ethnic donors, it establishes transcriptional baselines from bladder mucosa to vascular endothelial cells using unified scRNA-seq protocols.

C Experimental Details

C.1 Pre-Training Details

The scMMGPT model employs a multimodal pre-training framework that integrates gene expression data with textual information. Inheriting scGPT's (Cui et al., 2024) architecture, the cell encoder utilizes a gene vocabulary of 60,697 entries. For cellular input representation, we implement a top-value alignment strategy that selects the 2,048 highest-expressed genes along with their expression values. Cross-modal alignment is achieved through a Q-Former (Li et al., 2023) module with 32 query tokens, where the cross-attention mechanisms are activated every two layers.

Pre-training was executed on eight NVIDIA 4090D GPUs over five epochs (1.4 million total steps), requiring approximately five days for completion. The optimization process employed AdamW with a weight decay of 0.001 and a peak learning rate of 10^{-5}, modulated through a linear warmup (1,000 steps from 10^{-6} minimum learning rate) followed by linear decay. We select 2 negative samples for each sample to calculate the InfoNCE (Oord et al., 2018) loss.

Table 8: Model architecture specifications

Parameter	Value
Gene vocab size	60,697
Gene padding function	High value
Gene padding max len	2,048
QFormer BERT hidden dim	768
QFormer num_query_token	32
QFormer cross_attention_freq	2
Gene embed dim	512
Cell projector dim	256
Text projector dim	256
Language model hidden size	2,048
LM output max length	128
Cell decoder attention layer	1
Cell decoder attention head	4

Table 9: Pre-training configurations

Parameter	Value
Similarity function	Cosine similarity
Optimizer	AdamW
Scheduler	Linear
Max learning rate	1e-05
Warm up steps	1000
Weight decay	0.001
Batch size	12

C.2 Downstream Training Details

For the fine-tuning of downstream tasks, we conduct single-epoch training with a constrained batch size of 4, preserving the AdamW optimizer configuration in the pre-training stage. Language model adaptation employs Low-Rank Adaptation (LoRA) (Hu et al., 2022) with a rank-decomposition dimension r of 8, a scaling factor α of 32, and a dropout ratio of 0.1 for stochastic regularization during weight adaptation.

For each downstream analysis dataset, we perform quality control by removing the ambiguous categories (e.g., ”Other”, ”Unknown”). We establish symmetrical training pairs with strict 1:1 allocation between cellular generation and textual synthesis objectives. This balanced design promotes bidirectional cross-modal alignment while mitigating task dominance.

C.3 Metric Details

For the evaluation of cell clustering, we use both biological conservation metrics and batch correction metrics (Luecken et al., 2022). All the metrics are the higher the better.

Biological conservation metrics:

- **NMI$_{\mathbf{cell}}$** (Normalized Mutual Information): This metric measures the similarity between predicted clusters and ground-truth cell type labels.
- **ARI$_{\mathbf{cell}}$** (Adjusted Rand Index): This metric measures the agreement between clustering results and true labels, adjusted for chance groupings.
- **ASW$_{\mathbf{cell}}$** (Average Silhouette Width for cell types): This metric measures how well each cell fits within its assigned cluster compared to other clusters.
- **Avg$_{\mathbf{bio}}$**: The average of the three biological conservation metrics NMI$_{\text{cell}}$, ARI$_{\text{cell}}$ and ASW$_{\text{cell}}$.

Table 10: Ablation study on the ratio of positive/negative samples.

Micro Batch Size	Negative Samples	**Myeloid**		**hPancreas**		**Multiple Sclerosis**		**PBMC-3K**	
		Accuracy	F1	Accuracy	F1	Accuracy	F1	Accuracy	F1
3 (default)	2 (default)	**69.45**	65.62	**94.97**	**71.19**	87.12	**83.25**	94.72	91.84
6	5	68.25	**65.74**	91.28	68.27	86.45	82.73	94.61	91.07
12	11	66.68	65.04	86.84	62.61	**87.6**	82.7	**95.04**	**92.55**

Batch correction metrics:

- **ASW$_{\textbf{batch}}$** (Average Silhouette Width for batches): This metric measures the mixing of batches, where a lower silhouette score indicates better integration across batches.
- **Graph$_{\textbf{conn}}$** (Graph Connectivity): This metric measures how well cells from the same batch are connected in the nearest neighbor graph, indicating successful batch correction.
- **Avg$_{\textbf{batch}}$**: The average of the two batch correction metrics ASW$_{\text{batch}}$ and Graph$_{\text{conn}}$.

D Addictional Experiment results

D.1 Ablation Study on the Ratio of Positive/Negative Samples

For the contrastive objective, the construction of positive and negative samples can affect the training dynamics. We vary the ratio between positive and negative samples by changing the micro-batch size and the number of negative samples. As shown in Table 10, different settings achieve the best performance on different benchmarks, while the overall differences remain moderate. This suggests that our method is robust to the positive/negative sampling ratio.

D.2 Text-guided Pseudo-Cell Generation

We conduct cell generation experiments on the immune tissue (Domínguez Conde et al., 2022) dataset. We select several generative single-cell models as baselines, including scGen (Lotfollahi et al., 2019), scVI (Lopez et al., 2018), scDiffusion (Luo et al., 2024a), scGPT (Cui et al., 2024), and C2S (Levine et al., 2024). Inspired by previous studies, we train a simple k-Nearest Neighbors (k-NN) classifier on the test set to distinguish the generated cells. The classification accuracies under different k values are reported to reflect the quality of the generated cells.

The results are presented in Table 11. scMMGPT achieves state-of-the-art performance in text-conditioned pseudo-cell generation, significantly outperforming all baseline models across all k-NN accuracies (k=3,5,10,25). The consistently high accuracy and low standard deviations of scMMGPT demonstrate its robustness and effectiveness in bridging cellular and textual data.

Table 11: Results of text-conditioned pseudo-cell generation on the immune tissue dataset. The baseline results are borrowed from (Levine et al., 2024).

	k-NN Accuracy			
Model	$k = 3$	$k = 5$	$k = 10$	$k = 25$
scGEN (Lotfollahi et al., 2019)	0.2376 ± 0.0112	0.2330 ± 0.0093	0.2377 ± 0.0053	0.2335 ± 0.0041
scVI (Lopez et al., 2018)	0.2436 ± 0.0062	0.2400 ± 0.0064	0.2425 ± 0.0034	0.2348 ± 0.0032
scDiffusion (Luo et al., 2024a)	0.2335 ± 0.0125	0.2288 ± 0.0111	0.2368 ± 0.0067	0.2306 ± 0.0049
scGPT (Cui et al., 2024)	0.1838 ± 0.0086	0.1788 ± 0.0169	0.1811 ± 0.0149	0.1882 ± 0.0071
C2S (Levine et al., 2024)	0.2588 ± 0.0061	0.2565 ± 0.0060	0.2746 ± 0.0073	0.2715 ± 0.0070
scMMGPT	**0.2996 ± 0.0065**$^{+0.04}$	**0.2992 ± 0.0055**$^{+0.04}$	**0.2986 ± 0.0038**$^{+0.02}$	**0.2981 ± 0.0051**$^{+0.03}$

D.3 Robustness in Cell Type Annotation

During the inference of cell type annotation, we combine the cell-text constructive InfoNCE loss and cell-text matching CE loss to get the type probability: $\lambda\mathcal{L}_{\text{InfoNCE}} + (1-\lambda)\mathcal{L}_{\text{CE}}$ (§3.4). In this case, the choice of λ may influence the downstream annotation performance. We conduct inference on different levels of $lambda$ to test scMMGPT's robustness, and the results are shown in Table 12.

Table 12: The impact of lambda setting on our model.

	Myeloid		**hPancreas**		**Multiple Sclerosis**		**PBMC-3K**	
λ	Accuracy	F1	Accuracy	F1	Accuracy	F1	Accuracy	F1
0	**68.96**	**67.57**	97.58	80.52	87.28	83.8	94.29	92.92
0.01	68.79	67.49	97.56	80.48	87.29	83.87	94.29	92.92
0.05	67.71	65.5	97.56	81.06	87.4	83.93	94.4	92.98
0.1	67.01	64.15	**97.63**	**81.49**	87.35	83.91	94.4	92.98
0.2	65.81	62.76	97.51	80.54	87.35	83.85	94.4	93.07
0.3	64.96	61.55	97.41	80.45	87.33	84.38	94.72	93.45
0.4	64.5	60.77	97.44	80.46	87.38	84.49	94.72	93.45
0.5	64.29	60.24	97.41	80.42	87.42	**84.5**	94.72	93.45
0.6	64.12	59.93	97.41	80.52	**87.43**	83.95	94.72	93.45
0.7	63.77	59.54	97.41	80.72	87.39	83.83	**94.83**	**93.51**
0.8	63.45	59.24	97.41	80.72	87.42	83.53	94.83	93.51
0.9	63.39	59.2	97.39	80.68	87.38	83.24	94.83	93.51
0.95	63.33	59.12	97.39	80.68	87.38	81.67	94.83	93.51
0.99	63.24	59.05	97.39	80.68	87.38	81.67	94.83	93.51
1	63.24	59.05	97.39	80.68	87.37	81.66	94.83	93.51

E Visualization

E.1 Effectiveness of Different Cell Representation Methods

To further quantify the information loss in cell sentences, we conduct a visualization experiment comparing cell sentence inputs with original expression values. Specifically, we train two separate MLPs with identical hyperparameters for cell type annotation on the PBMC-10K (Gayoso et al., 2022) dataset. As shown in Figure 3, the cell sentence representation leads to a significant increase in error rate, particularly when distinguishing morphologically similar cell types such as dendritic cells and FCGR3A+ monocytes. This finding highlights the non-negligible cellular information lost during the transformation from numerical expression levels to cell sentences, which limits the effectiveness of related models in downstream applications.

E.2 Batch Effect Mitigation in scMMGPT Embeddings.

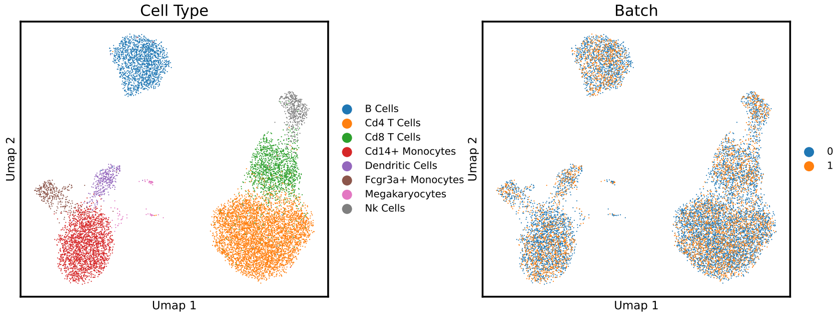

Figure 7: UMAP visualization of scMMGPT's embeddings for cells from different experimental batches on PBMC-10K (Gayoso et al., 2022). The result demonstrates the model's ability to capture cell type distinctions while effectively mitigating batch effects.

In wet lab experiments, it is challenging to maintain identical experimental conditions across different batches, which can lead to variations in the measured scRNA-seq data. We compute scMMGPT embeddings on PBMC-10K and visualize them using UMAP, as shown in Figure 7. The results demonstrate that cell embeddings from scMMGPT effectively capture cell type differences while minimizing the influence of batch effects.

E.3 Biological Signals in scMMGPT Embeddings

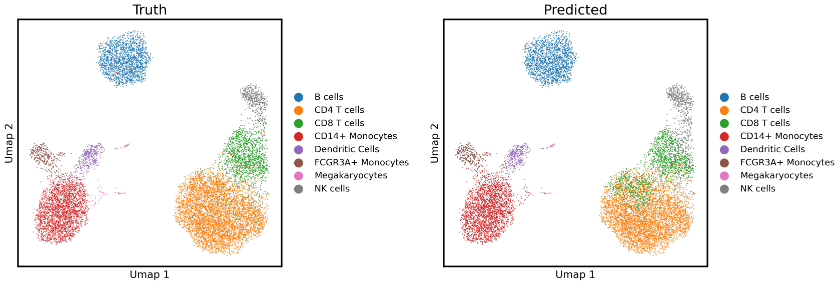

Figure 8: UMAP plot of embeddings from scMMGPT for PBMC-10K (Gayoso et al., 2022) dataset in zero-shot task. Plots are colored by actual cell type labels and predicted cell type labels.

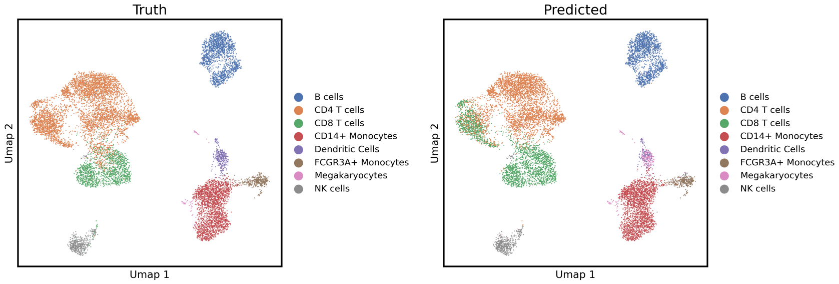

Figure 9: UMAP plot of embeddings from LangCell (Zhao et al., 2024) for PBMC-10K (Gayoso et al., 2022) dataset in zero-shot task. Plots are colored by actual cell type labels and predicted cell type labels.

We perform visualization on the PBMC10K dataset to show the cell embedding quality of scMMGPT (Figure 8). We also visualize the embeddings from the LangCell model (Figure 9) for comparison. In the plots, cells of the same type cluster closely together. When we compare the truth labels and predicted labels, we find that scMMGPT can correctly annotate most cells without fine-tuning.

E.4 Detailed descriptions for metrics in Figure 1.

In this section, we provide detailed descriptions and sources for each metric presented in Figure 1. Models not evaluated on a specific metric are represented by 0.

- **Myeloid, hPancreas, Multiple Sclerosis, PBMC-3K:** Data sourced from Table 1. We report the F1 score of each model for the cell type annotation task on these datasets.
- **PBMC-10K, Covid-19:** Data sourced from Table 2. We report the Avg_{bio} of each model for the Cell cluster task.
- **Immune Tissue:** Data sourced from Table 11. We report the F1 score of each model for the cell description generation task on the Immune Tissue dataset.
- **Tabula Sapiens:** Data sourced from Table 6. We report the Acc@1 of each model on the Tabula Sapiens dataset under the ”Fine-tuned on 30% Types” condition.
- **IT Gen:** Data sourced from Table 11. We report the 3-NN Accuracy of each model for the text-conditioned pseudo-cell generation task on the Immune Tissue dataset.

E.5 Heatmap of Cell Type Annotation result

In this section, we show heatmaps of confusion matrices across different cell-type annotation datasets. We normalize each cell type to provide a clear and consistent view of the accuracy of the model. As

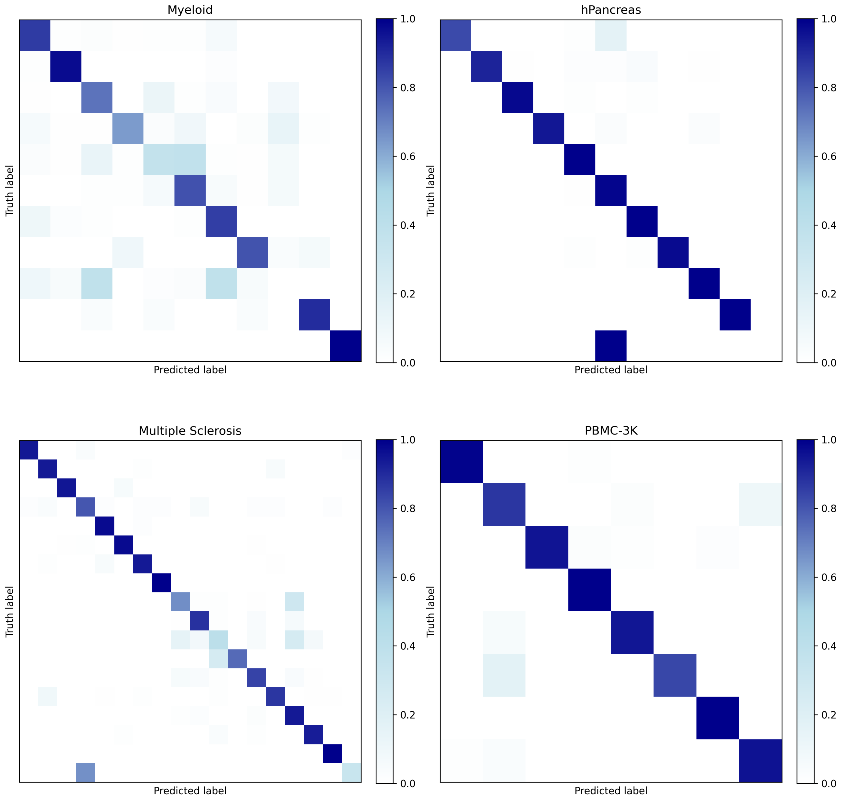

Figure 10: Heatmap of the results from scMMGPT's Cell Type Annotation on Myeloid (Cheng et al., 2021), hPancreas (Chen et al., 2023), Multiple Sclerosis (Schirmer et al., 2019) and PBMC-3k (Zheng et al., 2017) dataset.

shown in Figure 10, a clear diagonal line is visible in each heatmap, showing that our model achieves high prediction accuracy in all datasets.

E.6 Visualization of scRNA-seq Data.

To facilitate a better understanding of scRNA-seq matrices, we select a subset of cells from the Tabula Sapiens dataset for visualization. In wet-lab single-cell sequencing experiments, researchers measure the expression levels of a predefined set of genes across individual cells. Each value in the matrix represents the expression level of a corresponding gene within a single cell. The colors in the heatmap indicate the log1p-transformed expression levels.

E.7 Cell-Text Similarity Matrix for All Cell Types

We visualize the cell-text similarity matrix across all cell types from multiple tissues, including blood, heart, brain, kidney, lung, pan-cancer, and pancreas. As shown in Figure 12, cell-text pairs from the same tissue exhibit higher similarity, indicating that our representations capture tissue-specific biological semantics. Moreover, the diagonal entries achieve the highest similarity scores, suggesting that each cell type is most similar to its corresponding text description.

F Licenses for existing assets

In this section, we discuss the licenses and terms of use of the open-sourced assets involved in the development of scMMGPT.

- The CellxGene database is protected under CC-BY 4.0 license.
- The code and checkpoints of scGPT are under the MIT license.

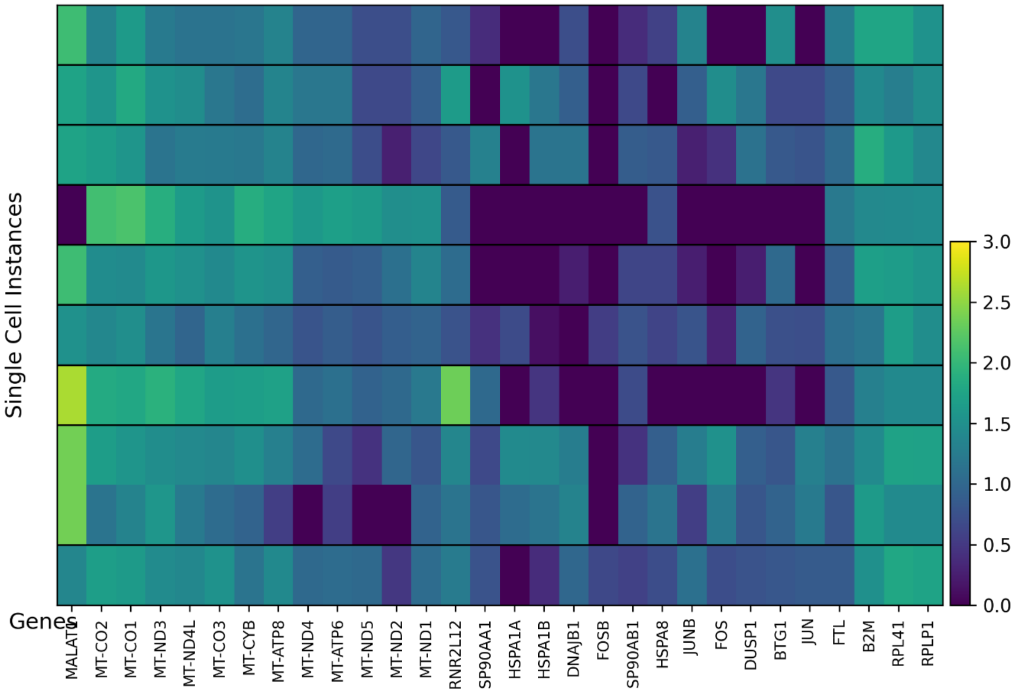

Figure 11: Visualization of a single-cell RNA sequencing matrix. Rows represent individual cells, and columns represent genes. The color intensity corresponds to the log1p-transformed expression levels, with darker shades indicating higher expression.

- The checkpoints of BioMedBert (Gu et al., 2021) are under the MIT license.
- The llama 2 series models are under the llama2 license.

The assets of this work are under the CC BY-NC license.

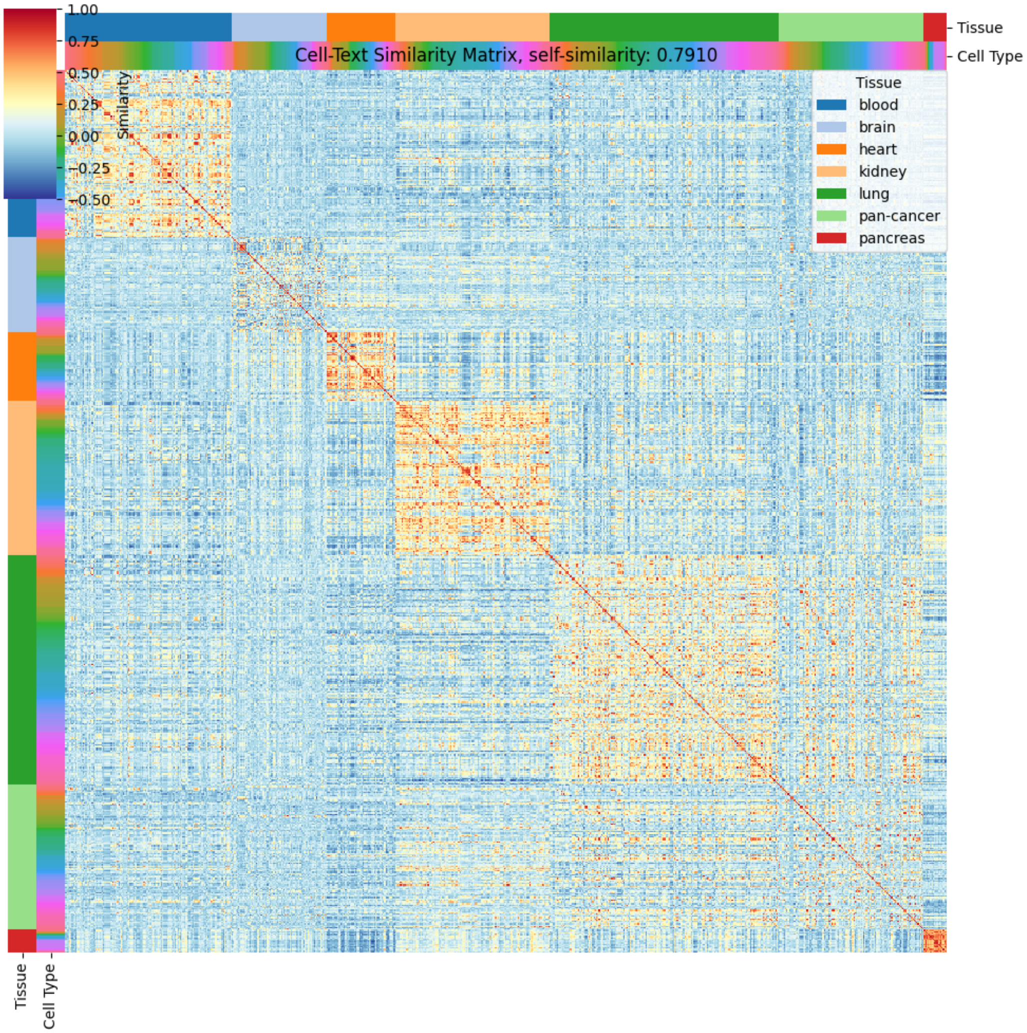

Figure 12: Cell-text similarity matrix for all cell types across blood, heart, brain, kidney, lung, pan-cancer, and pancreas tissues. Higher similarity is observed within the same tissue, and the diagonal exhibits the highest cell-text similarity.